ELSEVIER

Journal of Archaeological Science 34 (2007) 1064–1077

Journal of Archaeological SCIENCE

http://www.elsevier.com/locate/jas

Hayonim Cave: a TL-based chronology for this Levantine Mousterian sequence

N. Mercier [a,*], H. Valladas [a], L. Froget [a], J.-L. Joron [b], J.-L. Reyss [a], S. Weiner [c], P. Goldberg [d], L. Meignen [e], O. Bar-Yosef [f], A. Belfer-Cohen [g], M. Chech [h], S.L. Kuhn [i], M.C. Stiner [i], A.-M. Tillier [j], B. Arensburg [k], B. Vandermeersch [j]

[a] *Laboratoire des Sciences du Climat et de l'Environnement-IPSL, UMR CEA-CNRS-UVSQ, Domaine du CNRS, avenue de la Terrasse, 91198 Gif-sur-Yvette, France*
[b] *Laboratoire Pierre Süe, Groupe des Sciences de la Terre, CEN Saclay, 91191 Gif-sur-Yvette, France*
[c] *Weizmann Institute of Science, Structural Biology Department, 76100 Rehovot, Israel*
[d] *Boston University, Department of Archaeology, 675 Commonwealth Avenue, Boston, MA 02215, USA*
[e] *Centre d'Etudes, Préhistoire, Antiquité, Moyen Age, UMR 6031 du CNRS, 250 rue Albert Einstein, 06560 Valbonne, France*
[f] *Harvard University, Peabody Museum, 11 Divinity Avenue, Cambridge, MA 02138, USA*
[g] *Institute of Archaeology, The Hebrew University, Mount Scopus, Jerusalem, Israel*
[h] *MNHN, Laboratoire d'Anthropologie, Musée de l'Homme, 17 place du Trocadéro, 75116 Paris, France*
[i] *University of Arizona, Department of Anthropology, Building 30, Tucson, AZ 85721-0030, USA*
[j] *Laboratoire d'Anthropologie des Populations du Passé, UMR5199-PACEA, Université Bordeaux 1, avenue des Facultés, 33405 Talence, France*
[k] *Department of Anatomy and Anthropology, Sackler School of Medicine, Tel Aviv University, Ramat Aviv 61108, Israel*

Received 1 April 2005; received in revised form 12 December 2005; accepted 27 September 2006

Abstract

The thermoluminescence dating method was applied to 77 heated flints from the Mousterian layers of Hayonim Cave in order to provide a precise TL-based chronology for this important Levantine sequence. A detailed dosimetric study was performed by using 76 dosimeter capsules and revealed strong spatial dose-rate variations. In parallel, Fourier transform infrared spectrometry enabled the identification of various mineral assemblages in the sediments of the cave and to localize the boundaries of these assemblages. By comparing these two data sets, it is shown that low dose-rate values (~500 μGy/a) are systematically recorded in areas where the calcite-dahllite (CD) assemblage is preserved, whereas higher values (up to 1300 μGy/a) are associated with the leucophosphite, montgomeryite, variscite and siliceous aggregates (LMVS) assemblage. The dosimetric and mineralogical information was combined in order to assess, where possible, the dose-rate experienced by each flint during its burial. Some of the flint samples analyzed were too close to mineral assemblage boundaries and were therefore discarded. This rigorous selection led to TL ages ranging from 230 to 140 ka for the lower part of the Mousterian sequence (layers F and Lower E), which contains lithic industries characterized by blade production using the laminar method.

Keywords: Thermoluminescence dating; Mousterian; Chronology; Near-East; Hayonim Cave

1. Introduction

Hayonim Cave is located in the western Galilee, Israel, on the right bank of Nahal Meged (Fig. 1). The cave was formed by karstic activities in an Upper Cretaceous limestone reef and is characterized by a huge arch providing access to several chambers, one of which is open to the outside by means of a 25-m-high chimney. The sedimentary infilling is at least 6 m thick and is mainly of anthropic origin (Goldberg and Bar-Yosef, 1998); the sediments contain remains of combustion products (charcoal, ash remnants and phytoliths …), lithic

* Corresponding author.
E-mail address: Norbert.Mercier@lsce.cnrs-gif.fr (N. Mercier).

0305-4403/$ - see front matter © 2006 Elsevier Ltd. All rights reserved.
doi:10.1016/j.jas.2006.09.021

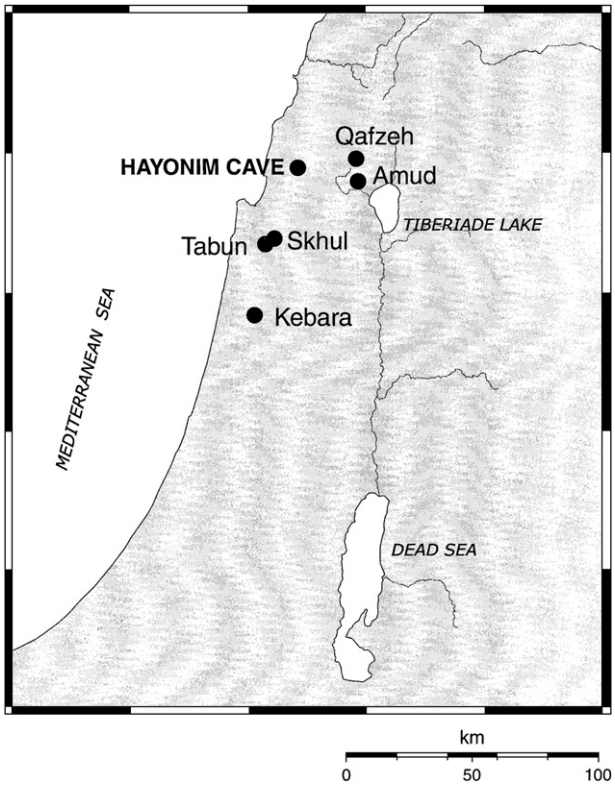

Fig. 1. Location of some Near-Eastern Middle Palaeolithic sites, including Hayonim Cave.

materials and bone residues from both large (gazelles, fallow deer, aurochs) and small (tortoises, lizards and rabbits) animals (Stiner, 2006; Stiner et al., 2000). The sequence is divided into several layers, from G (bottom) to A (top), containing a succession of occupations representing Middle Palaeolithic, Upper Palaeolithic and Natufian periods (Bar-Yosef, 1991; Bar-Yosef et al., 2006).

The excavations carried out between 1992 and 1999 were confined to two distinct locations within the site, the Central Area and the Deep Sounding, and mainly focused on the Mousterian sequence. During these excavations, the otherwise homogeneous Mousterian deposits of Layer E could be subdivided on the basis of lithic densities in order to evaluate chronological changes in the history of human occupation of the cave.

In Layer F and in the lower part of Layer E (units 6–4), the association of Levallois debitage with true blade technology (Laminar debitage) provides a specific aspect to this industry (Meignen, 1998, 2000). Characterized by the presence of elongated products (blades and points, often retouched) together with short often triangular Levallois blanks, the lithic assemblages closely resemble the material found in Abou Sif (Neuville, 1951). Generally speaking, they show global affinities in their core reduction strategies with the assemblages classically labelled as ‘‘Tabun D type’’ or Early Levantine Mousterian found in several sites throughout the Near East, even if the tool-kits show some variations. In contrast, in the Upper E assemblages (units 1–3), Levallois technology is clearly oriented towards the production of short and thin flakes (Meignen, 1998). Core management is evidenced by the presence of centripetal and unidirectionnal removals resulting in oval, quadrangular and subtriangular blanks. Retouched tools include mainly side-scrapers on large Levallois blanks. By all these criteria, the Upper E assemblages (especially units 1 and 2, with centripetal core preparation) show some affinities with the so-called ‘‘Tabun C type’’ industries found, for example, in Tabun unit I (Jelinek, 1981), in most layers from Qafzeh (Hovers, 1997) and Ksar Akil XXVI (Marks and Volkman, 1986). In fact, the preliminary technological study of these Upper E assemblages once more illustrates the variability and flexibility of the Levallois technology, resulting in an array of products of controlled morphology (Meignen, 1998).

Zooarchaeological analyses of the ungulate remains in Mousterian Layer E indicate that large animals were obtained by hunting, and prey biomass comparisons demonstrate that large game were the principal sources of meat, supplemented by modest quantities of tortoises and other slow-moving small animals (Stiner, 2006). The results also indicate significant expansion in human dietary breadth immediately following the Mousterian, and predator pressure on tortoise populations implies subtle increases in human population densities around the time of the Middle to Upper Paleolithic transition (Stiner et al., 2000). Human populations of the early Middle Paleolithic appear to have been small and widely dispersed, accounting for the relatively ephemeral nature of the Mousterian occupations at Hayonim Cave in contrast to those documented for the late Middle Paleolithic at Kebara Cave (Bar-Yosef, 1998; Stiner, 2006).

The few Middle Paleolithic hominid remains recovered at Hayonim Cave were concentrated in the central area of the cave (except for one specimen discovered in the entrance area) and the majority of them originated from upper stratigraphic units of layer E. To date, the fossil hominid record from other Mediterranean Levantine sites (i.e. Amud, Geula, Kebara, Qafzeh, Skhul, and Tabun) provides evidence that Mousterian assemblages can be associated with distinct human groups. In the past decade, there have been contradictory opinions expressed on the interpretation of anatomical differences between these fossil hominids and especially on the taxonomic designation of the Amud, Kebara and Tabun individuals (e.g. Arensburg, 2002; Arensburg and Belfer-Cohen, 1998; Hovers et al., 1995; Mann, 1995; Rak, 1998; Tillier, 1998; Tillier et al., 2003; Trinkaus, 1995; Vandermeersch, 1995). A major difference between the fossil record from the above-mentioned sites and that from Hayonim site lies in the fact that the latter has a low density of hominid remains and is dominated by isolated specimens (fragmentary skull remains, isolated teeth, cervical vertebra, hand and foot bones, parts of long bones) that are not suitable for precise taxonomic assignment (Arensburg et al., 1980; Arensburg et al., 1990). Moreover, in contrast with other Levantine sites, Hayonim Cave provides no evidence for mortuary practices within the Mousterian sequence.

2. Chronometric dating at Hayonim Cave

The chronology of the Hayonim Mousterian sequence has attracted much attention during the last two decades. Comparisons of micro-faunal remains with other Levantine

archaeological sequences (Tchernov, 1988; Tchernov, 1998) indicated that the faunal assemblages from Upper E in Hayonim Cave predated those discovered in Qafzeh Cave. Absolute dating methods have also been applied extensively: the U-series method was applied to a speleothem unearthed from the Mousterian deposits and provided the first reliable date (Schwarcz et al., 1980). Optical dating of sediments was attempted (Godfrey-Smith, personal communication) and preliminary results were obtained from the Thermoluminescence (TL) study of burnt lithics (Valladas et al., 1988). In parallel, the Electron Spin Resonance (ESR) dating method was applied to tooth enamel (Schwarcz and Rink, 1998). More recently, combined ESR/U-series analyses yielded detailed radiometric information indicating that the age of the Upper E Mousterian layer is around 180 ka, and not younger than 155 ka (Rink et al., 2004).

In this paper, we report the results of a study initiated 10 years ago whose aim was to provide a TL-based chronology for the Hayonim Mousterian sequence. A total of 77 age estimates obtained on heated flints is presented with associated radiometric information. Particular attention is given to environmental dose-rate variations through space and time, and to their possible correlations with the distribution of authigenic minerals formed as a result of diagenetic processes (Weiner et al., 2002). It is shown how these data can be combined in order to discard some TL results and to increase the reliability of the remaining TL ages.

3. Samples and methods

During the last 30 years, the TL method has been extensively used for the dating of burned flints discovered in archaeological sites, in particular those sites beyond the range of radiocarbon (Huxtable and Aitken, 1988; Mercier et al., 1991, 1995a,b,c, 2000; Valladas et al., 1986, 1987, 1988, 1998). The utility of the method is based on the fact that flints behave as excellent natural dosimeters which record doses delivered by the different types of radiation coming from the decay of radioisotopes, such as the U- and Th-series and potassium. The TL method is based on dosimetric measurements of these ionizing radiations. Short-ranged α and β particles ($\sim$20 μm and $\sim$2 mm, respectively) emitted from radioisotopes within the flint itself, provide an ''internal dose''. An ''external dose'' from long range ($\sim$40 cm max.) γ-rays (as well as from cosmic radiations) necessitate consideration of the immediate environment of the flints.

3.1. Burnt flint specimens and dosimetric measurements

More than 100 flint artefacts showing signs of heating were selected during the excavation campaigns at Hayonim Cave. The sample preparation followed the protocol defined by Valladas (1992). After the outermost 2 mm of each flint were removed, the remaining core was crushed and subjected to chemical treatment and its TL emission was analyzed. Only 77 flints had been heated at temperatures sufficient to ensure a complete resetting of the TL signal, and only these were selected for further analyses. Fig. 2 shows the TL emissions of sample (HAY 7) as well as the equivalent dose (ED). The natural and regenerated growth curves are typical of the sub-linear behavior observed for most of the Hayonim samples. These samples come from the Deep Sounding (squares D-E-F-28-27-26), and from the southern (squares I-J-K-24-23-22) and northern parts (squares G-H-I-J-20-19-18) of the Central Area of the excavations (Fig. 3).

As the excavations covered a relatively large area ($\sim$23 m^2), great effort was made to obtain detailed information on spatial variations in environmental dosimetry. A total of 76 calcium sulfate dosimeters were placed in different sections of the cave and remained in place for approximately 1 year. Most of them were inserted horizontally in the newly exposed profiles close to squares containing numerous burnt flints: G18, H19 and I20 – North section; K23-24 and I24 – South section and, in the Deep Sounding: squares D-E-F27 and F28. A few dosimeters were also inserted vertically at the end of the field season in squares where excavation was scheduled in subsequent years (see Fig. 3). Additional dosimetric countings were carried out on-site using a portable γ-detector inserted in natural holes

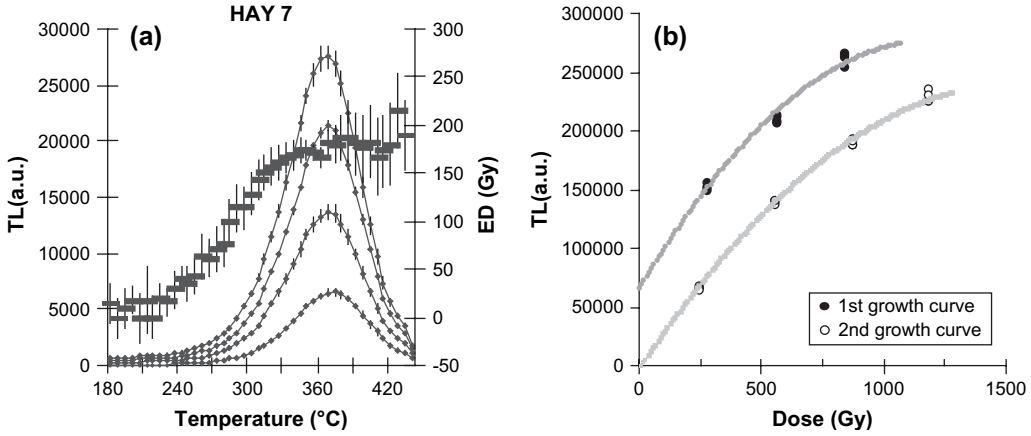

Fig. 2. (a) TL emission of sample HAY 7 for doses: 0, 281, 562, 843 Gy. The equivalent dose (ED) calculated as a function of temperature (''plateau test'') is indicated. (b) Growth curves for sample HAY 7 (natural + given doses (1) and regenerated (2)) are typical of the sub-linear behavior observed for most of the Hayonim samples.

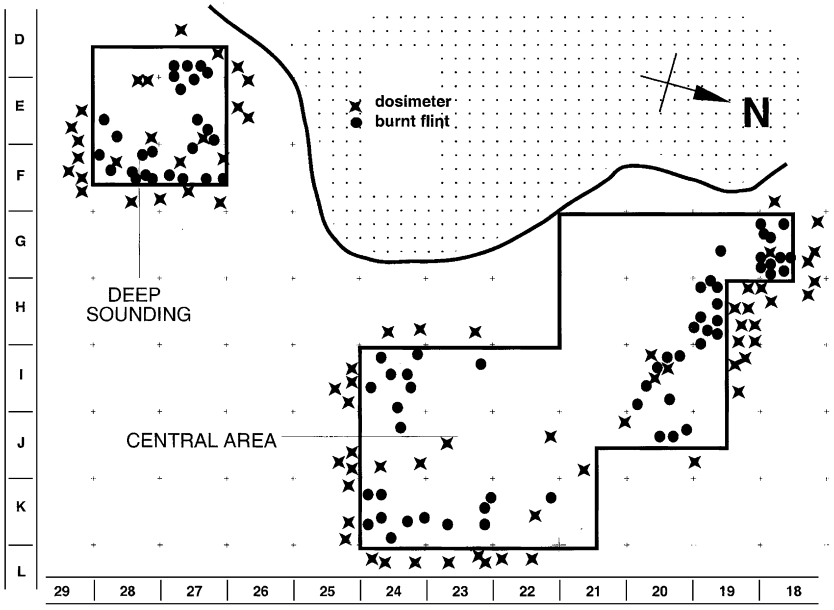

Fig. 3. Schematic map of Hayonim Cave showing boundaries of excavations, the Deep Sounding and the Central Area. The location of the dosimeters and flints are indicated with crosses and circles, respectively.

(burrows) present in some profiles, a few other measurements were made in the laboratory with a high purity germanium detector. In this case, about 100 g of sediment were analyzed by γ-spectrometry for obtaining information on possible disequilibria in the radioactive decay chains and investigating the repartition of the γ dose-rate between the U- and Th-series and potassium.

3.2. Fourier Transform Infrared analyses of sediments

Mineralogical analyses were carried out on-site during the excavation of Hayonim Cave using Fourier transform infrared (FTIR) spectroscopy in order to better understand the archaeology via sediment diagenesis and site formation processes (Weiner et al., 2002). This method is capable of identifying mineral assemblages using only a few tens of micrograms of sample (Weiner et al., 1993). More than 2100 samples were analyzed. It was shown that three major mineral assemblages are present in the archaeological assemblages at Hayonim: the first, termed CD (Weiner et al., 2002), is composed mainly of calcite and secondarily of dahllite. Calcite is the main residue of the fresh ash which originally made up the bulk of the sediments (Schiegl et al., 1994). Dahllite (also known as carbonated hydroxyapatite) results from interaction of calcite with phosphate-rich solutions. The second assemblage, termed LMVS, represents sediments that are more diagenetically altered. In the course of the diagenetic process, the dahllite dissolves and is replaced by other more stable phosphate minerals such as leucophosphite, montgomeryite and variscite. Due to the dissolution and transport of other minerals, the relative proportions of so-called siliceous aggregates and phytoliths, minor components in the original ash, increase with ongoing diagenesis. Note that the siliceous aggregates themselves, as well as one of the common authigenic phosphate minerals (leucophosphite) contain potassium (Schiegl et al., 1996). As noted above, the formation of the LMVS assemblage also results in the dissolution of bones which are composed of dahllite, a relatively unstable mineral with respect to the LMVS group. The third identified mineral assemblage consists of the most highly altered sediments, in which clays have broken down and silica has been released.

The extensive study of sediment mineralogy in the field also provided a detailed map of the spatial distribution of the three mineral assemblages. This map showed sharp variation in sediment mineralogy over distances as short as a few centimeters (Weiner et al., 2002; see their Figs. 10 and 11, for instance).

At this stage, it is interesting to notice that the local differences in sediment chemistry and rates of diagenetic activity, based on a combination of taphonomic methods and Fourier transform infrared (FTIR) spectroscopic analyses of sediment and bones (Stiner et al., 2001; Weiner et al., 2002), correlate closely with the distribution of bones in the sediments at Hayonim Cave. The quality of bone preservation follows an ‘‘all-or-nothing’’ pattern in the central area, with relatively abrupt changes in bone abundance rather than gradual transitions between good to poor preservation. The areas of good bone preservation are extensive and associate consistently with CD mineral assemblages dominated by calcite, dahllite or both. Bone preservation in Layer E was best within 2–3 m of the cave walls in the central area, especially between 420 and 500 cm below datum. Very few bones were preserved anywhere in Layer F, where secondary mineral assemblages (LMVS and altered clays) predominate in the sediments (Weiner et al., 2002).

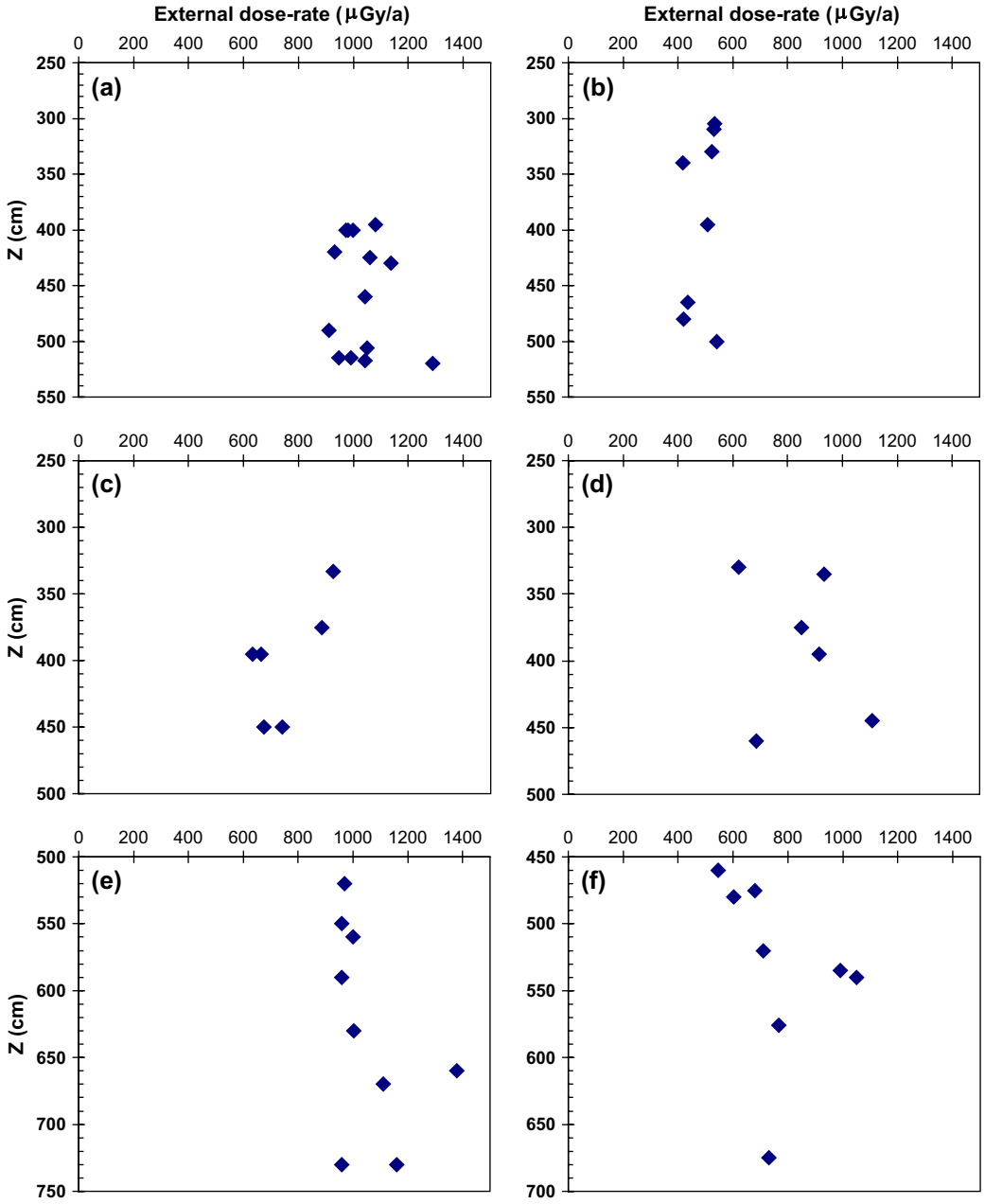

Fig. 4. Environmental dose-rates (μGy/a) measured with calcium sulfate dosimeters as a function of depth Z, for squares: (a) H19-G18; (b) L22-23-24; (c) I25-H23-24; (d) K-J25; (e) F27-28-29-E28-29 and (f) E26-D26-27-28. Note that for (a) and (b), the values are high (~1100 μGy/a) and low (~500 μGy/a), respectively, but do not vary significantly with depth. In contrast, for (c) and (d), the recorded dose-rates vary significantly, even on a relatively small scale (10–20 cm). In the Deep Sounding the values are around 1000–1200 μGy/a (e) or range from 500 to 800 μGy/a (f), but some are higher by ~30%.

4. Dosimetry results

4.1. Present-day environmental dose-rates

In Fig. 4 the environmental dose-rates recorded by the dosimeters are plotted as a function of depth. For simplification, they were grouped into nearby squares (a, H19-G18; b, L22-23-24; c, I25-H23-24; d, K25-J25 for the Central Area; e, F27-28-29-E28-29; and f, E26-D26-27-28 for the Deep Sounding). In squares H19-G18, the values are homogeneous, ranging from 900 to 1100 μGy/a (not including one value at ~1300 μGy/a) with 10% dispersion around the mean, and do not vary significantly with depth from $Z = 250$ to $Z = 550$ cm (Fig. 4a). The same trend with depth is observed for squares L22-23-24 (Fig. 4b), although the values are much lower (400–550 μGy/a). The range of variation in both profiles is about the same (~10%). On the other hand, the dose-rates can vary even over small differences of elevation in squares I25-H23-24 (Fig. 4c) and K25-J25 (Fig. 4d). In the Deep Sounding, significant variation also exist in squares E26-D26-27-28 (Fig. 4f) where dose-rates range from 500 to 1000 μGy/a. One can then conclude that in certain sections

of the cave, the environmental dose-rates do not vary significantly with depth over 1m or more, while in other parts, there are substantial variations at even small scales (<10 cm), horizontally and/or vertically.

These observations have direct implications for dating when dosimetric methods are used. We note that the range of the most energetic γ-rays (∼40 cm) is greater than the small-scale heterogeneity. Moreover present-day dose-rate measurements are seldom recorded at the precise locations where flint samples were collected, but at distances up to 1 m or more. This is not a problem in a homogeneous mineralogical environment where the dose-rate calculated by averaging the doses recorded in neighboring dosimeters should be representative of the dose-rate received by a sample in the same environment; in a heterogeneous mineralogical environment, however, the dose-rate values measured at different locations may differ significantly from the dose experienced by the sample. This fact clearly has to be taken into account when determining the environmental dose of a given sample.

4.2. Basis for the dosimetric heterogeneities

In the course of the field seasons, a general overview of the distribution of mineral assemblages in the cave and dose-rate values showed a strong correlation, as did the distributions of mineral assemblages and bone abundance. In sections where calcite and dahllite were abundant (CD assemblage), dose-rates around 500 μGy/a were recorded, whereas in sections rich in leucophosphite, montgomeryite, variscite and siliceous aggregates (LMVS assemblage), the dose-rates were significantly higher (up to 1300 μGy/a). In order to understand the basis for this correlation, sediment samples (∼300 mg) were taken from various sections, homogenized and the major minerals identified by FTIR. In parallel, neutron activation analysis (NAA) was performed on the remaining powder (∼250 mg) and the radioisotope contents (U, Th and K) were measured (Mercier et al., 1995). Fig. 5 gives the γ dose-rates calculated by assuming that the identified minerals were the only components in the environment (within a radius of at least 50 cm, i.e., greater than the typical range of the γ-rays). It is worth noting that the results basically confirm at a very small scale (the "scale" of a 300 mg sample) what was observed at a large scale: low dose-rates are associated with the CD assemblage (calcite and dahllite), and high dose-rates are associated with the assemblage made up of siliceous aggregates with varying quantities of leucophosphite and montgomeryite. The on-site survey with a gamma spectrometer also revealed that the lowest dose-rates (∼300 μGy/a) were measured from sediments dominated by calcite. Note too that Fig. 5 shows some exceptions, the most glaring being that one sample dominated by dahllite which has the third highest dose-rate. It should be noted that carbonated apatite has a tendency to readily occlude a variety of different ions, including apparently potassium.

These mineralogical data can also explain the variation in dose-rate observed along different profiles (Fig. 4). In mineralogically homogeneous sections, dose-rate values are fairly homogeneous: either low (∼500 μGy/a) as in squares L22-23-24 or high (∼1000 μGy/a) as in squares H19-G18. In areas where sharp mineralogical boundaries exist, the measured dose-rates have intermediate values depending on the relative distance of the dosimeters from these boundaries (see Weiner et al. (2002) for details on mineral assemblage distributions, and Aitken (1985) for dose-rate variations as a function of the relative distance). The implication of these observations to TL dating is that it is difficult, if not impossible, to reliably estimate a representative dose-rate for any burned flint samples located within 30 cm of a boundary between mineral assemblages. These samples cannot therefore be used for establishing a chronology.

4.3. Dose-rate changes with time

The NAA data can provide some insight into the basis of the dose-rate changes. Fig. 6a shows the distribution of the dose into the different components (the U- and Th-series and K-40). There is no obvious correlation between major mineral types and the source of radiation. As the samples are listed according to increasing radiation dose, one can however notice that high dose-rates are correlated with samples dominated by siliceous aggregates, which have high potassium contents (Schiegl et al., 1994, 1996). This is clearly demonstrated in Fig. 6b, which shows that the total γ dose-rate increases linearly as a function of the potassium content of the samples. Consequently, the contribution of the U- and Th-series to the annual dose-rate does not exceed 30–40%, except for a few samples.

As siliceous aggregates are only a minor component of fresh ash, samples dominated by siliceous aggregates must have undergone severe diagenesis resulting in the loss of the other components. This raises the important question of when this diagenesis occurred, as the timing could clearly affect the mean dose-rates experienced by the samples and consequently, the calculated ages. If, for example, the diagenesis

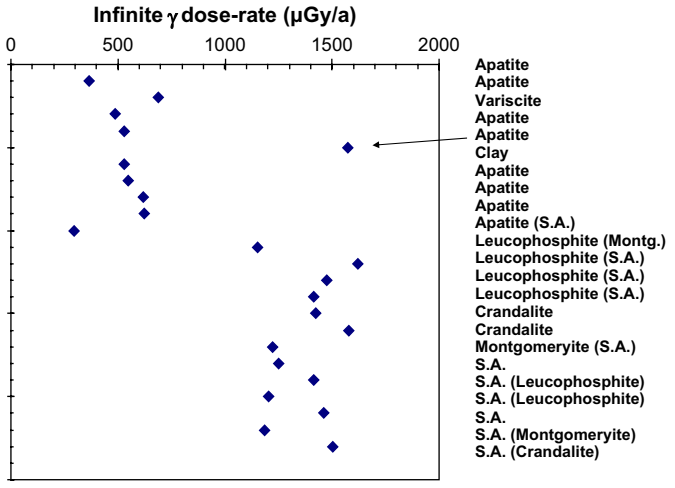

Fig. 5. Infinite γ dose-rates (μGy/a) for the different minerals identified by FTIR. For comparison, each value was computed by taking into account the U, Th and K contents determined by NAA and assuming that the identified mineral was the only component in the environment. The arrow indicates the exception mentioned in the text. (Carbonated hydroxyapatite (or Apatite) is used instead of Dahllite.)

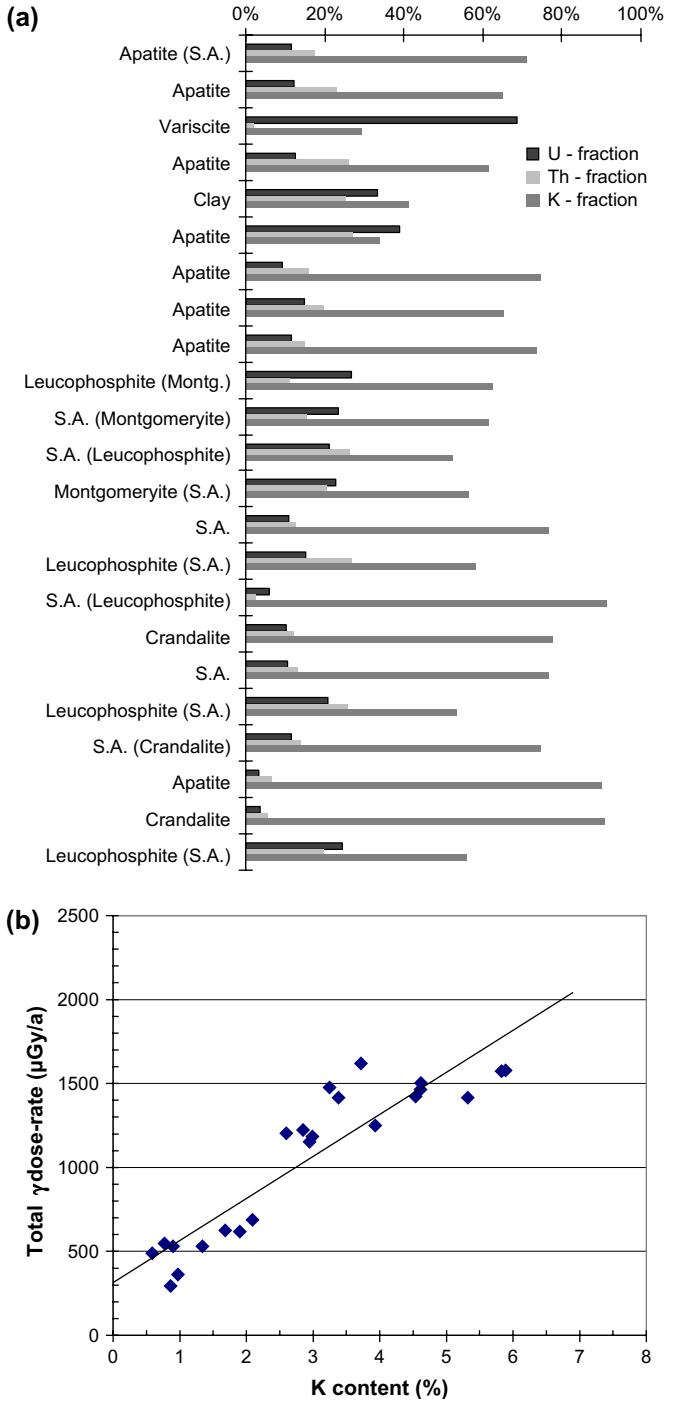

Fig. 6. (a) Contribution to dose-rate of the different components (the U- and Th-series and K-40). Note that the samples are listed from top to bottom with increasing total γ dose-rate. As no significant disequilibria have been detected in the 100 g sediment samples analyzed by γ-spectrometry in the laboratory, the listed γ dose-rates were calculated by taking into account all the γ-rays of the U- and Th-series. The second most abundant constituents are shown in brackets. S.A. refers to siliceous aggregates. (b) A plot of the total γ dose-rate as a function of the K content of the samples shows a linear correlation.

was a slow steady process that took place during most of the period of time that elapsed after the flint was deposited in the sediments, then using the present-day relatively high dose-rate would result in TL ages that are too young. If, on the other hand, the diagenesis took place soon after burial, this would not affect the TL ages as the dose-rate measurements today would be representative of the dose-rates experienced by the flints over most of the time since deposition.

Karkanas et al. (2000) and Shahack-Gross et al. (2004) have presented several lines of evidence all pointing to the conclusion that diagenesis in prehistoric caves in the Levant and in Greece, took place soon after burial, possibly even within hundreds or tens of years. One reason is that the diagenesis is driven mainly by the breakdown of organic material from bat and bird guano. This produces acids that in turn cause the dissolution of less stable minerals and the formation of more stable ones. So we assumed that the diagenetic history of the mineralogical assemblages in Hayonim Cave is not a major factor which induced changes in the dose-rates with time and so we used the present-day dose-rates to calculate the TL ages.

5. Thermoluminescence age estimates

5.1. Sample selection and results

As noted previously, the primary difficulty in evaluating the dose-rate for a given burned flint is related to its distance from a boundary between two mineral assemblages. For a sample unearthed from one of the two distinct environments (CD and LMVS assemblages) at a distance greater than 30 cm from an identified mineralogical boundary, the dose-rate was calculated by averaging the individual dose-rates recorded by the neighboring dosimeters in the same mineralogical environment. However, every sample located at a distance less than 30 cm from a boundary, as defined using the FTIR data, was noted and is identified with an asterisk (last column of Table 1), since the present-day environmental dose-rate it received just before it was unearthed cannot be determined with any reliability. The marked samples were then excluded from the discussion on the chronostratigraphy.

Table 1 lists 77 burnt flint samples from Hayonim Cave with their laboratory numbers, the layers and units in which they were discovered, their locations and relevant dosimetric data, as well as the estimated TL ages and associated errors. Details concerning the radiometric data and luminescence measurements are given in the legend of Table 1. All these TL ages are plotted in Fig. 7, as a function of stratigraphy. In general, it appears that the rejected samples (marked by an asterisk in Table 1 and open symbols in Fig. 7) have ages which are often scattered and in disagreement (older or younger) with those obtained for samples located in homogeneous dosimetric environments. Consequently, our methodology for selecting samples appears reliable and gives us confidence in the average ages listed below. However, this approach made us exclude several samples whose ages were in the same range as the others for the same layer.

5.2. Average ages

The selected samples (without an asterisk) were grouped into three sets depending on their location and their identified

Table 1
Analytical data and TL age estimates (all errors are given at one sigma level)

Sample lab. no.	Square, sub-square	Layer/unit	Location: (x,y,z) or depth (Z)	U (ppm)	Th (ppm)	K (%)	S-α μGy/10^3 α/cm^2	Dose rates						Equivalent dose		Age estimates	
								Internal		External		Total		Gy	±	ka	±
								μGy/a	±	μGy/a	±	μGy/a	±				
	G18	Northern part of Central Area															
21	d	2	(56,74,360)	0.48	0.07	0.07	15.2	263	19	921	102	1184	103	149	6	126	12
24	c	2	(64,27,386)	0.53	0.15	0.22	22.1	477	28	962	102	1439	106	183	16	127	14
23	d	2	(55,66,386)	0.92	0.14	0.10	12.4	424	26	982	102	1405	105	217	21	155	19
22	d	2	(70,87,394)	0.36	0.14	0.14	22.9	326	20	926	102	1251	104	149	9	119	12
62	c	2	(89,36,396)	0.70	0.14	0.08	11.6	316	19	977	102	1292	104	147	15	114	15
20	d	2	(89,74,396)	0.71	0.20	0.13	19.4	467	30	928	102	1395	106	204	10	146	13
27	d	2	(70,72,400)	0.43	0.21	0.11	18.5	314	21	937	102	1251	104	156	7	124	12
63	c	2	(77,43,409)	0.57	0.14	0.04	19.1	317	23	967	102	1284	104	161	11	125	13
26	d	2	(95,75,409)	0.51	0.14	0.07	15.1	279	17	937	102	1216	103	169	6	139	13
61	c	2	(84,36,411)	2.01	0.14	0.13	20.9	1144	87	923	102	2067	134	266	14	129	11
25	d	2	(60,72,418)	0.38	0.14	0.08	22.7	287	19	883	102	1170	104	147	6	125	12
	G19																
9	d	2	(53,62,402)	0.49	0.14	0.09	18.4	316	23	972	102	1288	104	153	4	119	10
	H19																
3	d	3	(90,80,390)	0.49	0.18	0.14	15.4	336	21	923	102	1259	104	181	13	144	16
5	d	3	(80,55,395)	0.86	0.17	0.12	18.2	511	38	932	102	1443	109	202	7	140	11
10	c	3	(70,26,395)	0.19	0.11	0.02	10.6	89	6	942	102	1031	102	153	11	148	18
11	d	3	385-400	0.82	0.08	0.15	20.0	530	37	946	102	1476	109	216	10	146	13
4	c	3	(61,29,399)	0.68	0.16	0.09	16.2	383	27	942	102	1325	106	189	8	142	13
7	c	3	(52,40,407)	0.56	0.25	0.16	15.4	382	25	942	102	1324	105	189	10	143	14
12	d	3	(75,53,467)	0.85	0.14	0.11	13.8	428	28	583	102	1011	106	170	6	169	19*
2	d	4	(95,80,505)	1.86	0.08	0.16	30.4	1387	125	410	102	1797	161	221	15	123	14*
8	d	4	490-510	0.29	0.15	0.06	17.7	192	14	413	102	605	103	102	4	168	29*
1	c	4	525-530	1.13	0.14	0.09	15.5	549	41	413	102	963	110	213	10	221	27*
	I20																
415	d	4	(95,95,465)	0.76	0.15	0.10	21.2	492	35	391	100	883	106	139	4	157	19
416	a	4	(48,2,463)	0.41	0.14	0.07	16.1	251	16	388	100	639	102	133	7	208	35
417	c	4	(58,25,463)	0.59	0.16	0.07	18.6	353	24	396	100	748	103	122	4	163	23
507	d	6	(63,58,514)	0.50	0.13	0.06	19.9	312	47	604	121	916	130	128	9	140	22*
508	c	6	(55,31,531)	0.76	0.18	0.12	16.9	448	47	610	121	1058	130	173	18	163	26*
515	b	6	(31,71,530)	0.37	0.10	0.04	21.1	236	47	613	121	849	130	160	17	188	35*
	J20																
501	a	5	(475/480)	0.37	0.21	0.10	25.5	330	47	484	121	814	130	105	6	128	22*
502	a	5	(495/500)	0.68	0.20	0.13	24.0	514	47	484	121	998	130	141	20	141	27*
503	a	5	(490/495)	0.70	0.09	0.04	20.6	395	47	484	121	880	130	140	10	159	26 *
	K22	Southern part of Central Area															
412	a	4	(10,15,460)	2.73	0.11	0.09	31.1	1960	169	384	100	2344	196	246	6	105	9
	K23																
72	a	1	(19,43,281)	0.91	0.15	0.15	22.1	617	42	506	71	1123	82	213	6	190	15*
69	d	1	(77,67,295)	0.48	0.15	0.09	19.4	328	21	429	61	757	64	161	14	213	26*

(*continued on next page*)

Table 1 (*continued*)

Sample lab. no.	Square, sub-square	Layer/unit	Location: (*x*,*y*,*z*) or depth (*Z*)	U (ppm)	Th (ppm)	K (%)	S-α μGy/10^3 α/cm^2	Dose rates						Equivalent dose		Age estimates	
								Internal		External		Total		Gy	±	ka	±
								μGy/a	±	μGy/a	±	μGy/a	±				
410	a	4	(7,37,457)	0.65	0.22	0.05	13.2	306	20	421	100	727	102	145	4	200	29
414	b	5	(22,73,466)	0.62	0.31	0.12	18.3	421	27	413	100	834	104	134	8	160	22
	K24																
71	b	1	(17,57,289)	0.58	0.13	0.10	22.0	402	27	495	71	897	76	193	11	215	22*
74	b	2	(43,59,301)	1.18	0.13	0.14	22.2	758	55	493	71	1251	90	246	13	197	17*
67	d	2	(62,96,307)	1.12	0.22	0.13	28.3	848	69	501	101	1349	122	201	10	149	15
68	d	2	(72,62,310)	0.63	0.18	0.03	22.8	390	34	552	101	942	106	153	6	163	19
70	c	2	325-340	0.56	0.16	0.04	18.8	313	22	880	160	1192	162	217	8	182	26*
65	c	3	(82,37,351)	0.73	0.15	0.14	13.8	407	25	871	160	1278	162	207	11	162	22
401	d	4	(81,86,459)	0.69	0.15	0.09	20.2	425	32	660	101	1085	106	167	10	154	17
	J24																
84	a	3	(41,21,395)	0.72	0.22	0.11	28.6	579	45	834	130	1413	138	220	7	155	16
	I24																
76	b	3	(46,90,371)	0.76	0.24	0.13	23.8	563	43	711	101	1274	110	215	10	169	17
75	a	3	375-380	0.32	0.12	0.09	17.2	224	13	623	130	847	131	151	7	178	29
82	c	3	(62,42,395)	1.60	0.19	0.15	36.0	1383	140	614	101	1996	172	256	16	128	14
80	c	3	(75,20,399)	0.35	0.13	0.11	22.0	289	24	601	100	889	103	128	4	144	17
418	b	4	(10,52,454)	0.43	0.13	0.09	19.3	296	20	701	100	997	102	140	6	140	16
402	a	4	(24,1,456)	0.48	0.15	0.10	18.6	321	20	633	100	954	102	144	5	151	17
403	d	4	(80,57,458)	0.29	0.19	0.04	12.9	156	10	610	100	766	101	149	10	194	28
	I23																
413	a	4	(18,27,458)	1.89	0.12	0.14	33.1	1475	144	648	100	2123	175	233	20	110	13*
	D27	Deep Sounding															
56	b	C/E	(42,76,457)	0.94	0.12	0.10	13.2	442	29	601	101	1044	105	89	4	85	9*
52	b	C/E	(47,81,458)	0.45	0.17	0.08	20.8	312	22	604	101	916	103	188	8	206	25*
53	d	C/E	(76,81,496)	0.90	0.04	0.10	11.9	401	24	604	101	1005	104	273	12	272	30*
54	d	C/E	(61,71,510)	0.46	0.16	0.03	12.4	207	13	673	101	880	102	86	4	98	12*
55	d	C/E	(85,78,510)	0.45	0.22	0.11	19.7	336	23	626	101	962	103	34	1	35	4*
51	d	E base	(51,92,539)	1.83	0.12	0.04	31.0	1294	109	974	101	2267	148	195	9	86	7*
	E27																
58	b	E base	520-525	0.94	0.08	0.07	20.6	536	39	876	102	1412	109	279	15	197	18
50	b	F top	(45,62,545)	0.40	0.10	0.06	15.2	228	14	851	102	1078	103	253	14	235	26
60	b	F top	555-560	1.26	0.24	0.12	24.3	836	65	901	102	1737	121	355	17	204	17
57	c	F top	(76,14,578)	0.81	0.24	0.03	21.7	476	38	723	101	1199	108	269	8	224	21
	E28																
404	d	E base	(87,55,543)	0.48	0.12	0.14	20.0	366	27	915	101	1280	104	160	6	125	11*
409	d	E base	(80,70,558)	0.74	0.16	0.11	23.2	514	42	920	101	1434	109	227	5	159	13
	F28																
406	c	E base	(75,35,520)	0.80	0.07	0.08	28.1	573	47	710	121	1283	130	259	24	202	28
516	b	F base	(10,75,728)	1.43	0.08	0.07	22.9	844	47	1136	121	1980	130	406	64	205	35
522	a	F base	(23,5,719)	1.16	0.05	0.06	19.7	622	47	890	121	1513	130	344	20	227	24
523	d	F base	(67,60,726)	3.28	0.04	0.02	14.9	1354	47	1077	121	2431	130	547	94	225	41

524	a	F base	(26,14,715)	0.67	0.18	0.07	26.5	489	47	908	121	1397	130	255	80	183	60	
525	b	F base	(43,98,703)	1.14	0.05	0.05	17.8	558	47	1167	121	1725	130	433	13	251	20	
526	b	F base	(4,95,715)	0.83	0.07	0.07	20.6	480	47	1143	121	1623	130	303	21	187	20	
527	b	F base	(19,87,711)	0.61	0.19	0.08	18.3	371	57	1143	131	1514	143	334	11	221	22	
	F27																	
517	d	F base	(92,89,728)	1.60	0.07	0.07	23.0	935	47	1173	121	2108	130	462	6	219	14*	
518	d	Fbase	(54,60,733)	0.74	0.12	0.05	21.2	427	47	1167	121	1594	130	371	12	233	20	
519	b	Fbase	(47,77,718)	0.37	0.22	0.03	10.3	163	47	1132	121	1295	130	245	8	189	20	
520	d	Fbase	(74,98,718)	0.99	0.15	0.11	23.3	653	47	1162	121	1815	130	318	32	175	22	
521	b	Fbase	(21,99,736)	1.35	0.12	0.10	26.5	909	47	1104	121	2013	130	244	18	121	12*	

The U, Th and K contents of flints were measured by neutron activation analysis (NAA) at the Pierre Süe Laboratory, Saclay (Joron, 1974) and have each an error of 10%. The S-α sensitivity (Valladas and Valladas, 1982) was determined by comparing TL signals induced respectively by a β dose (Sr-90 source: dose-rate 8.2 Gy/min) and by α-rays from a Pu-238 source (flux 2.35×10^6 α/cm^2 per s). The internal dose rate was computed from the U, Th and K contents using published values of specific dose-rates (Liritzis and Kokkoris, 1992; Valladas, 1988) and the S-α sensitivity determined experimentally. The external dose-rate includes a cosmic contribution of 60 μGy/a (Prescott and Hutton, 1988). The TL signals were recorded with an automatic reader (Valladas et al., 1994): the blue component of the 380 °C TL peak was selected by a MTO 380 nm filter and detected with a EMI 9635QB photomultiplier tube. The heating rate was 5 °/s. ED values were determined by comparing the first and second TL growth curves (Mercier et al., 1992), since for most samples, the growth curve of the TL signal (TL versus acquired dose) was sub-linear whereas for the others, the shape was more linear. Typical examples of sub-linear growth curves are shown in Fig. 2. All the flints listed have passed the plateau test (Aitken, 1985). The errors associated with the age estimates were computed according to Aitken (1985, appendix B).

mineralogical assemblage: the northern part of the Central Area includes the squares G18-G19-H19-I20-J20; the southern part, the squares K22-K23-K24-J24-I24-I23 and the Deep Sounding, the squares D27-E27-E28-F28-F27. For each layer and unit within a specific area, the average TL age value was calculated (Table 2); since these layers do not represent single but successive occupations, the associated error was obtained by averaging the individual errors; in brackets, the standard deviation of the individuals results is also given. Note, however, that samples from square D27 (Deep Sounding) were all discarded because of the incoherence of the TL results, ranging from ~272 to ~35 ka (!). This may well be related to the presence of a 1.30-m-deep trench thought to be the product of water driven erosion which resulted in redeposition of younger sediments together with stone artefacts (Weiner et al., 2002).

Beginning with the bottom of the sequence, samples collected in the Deep Sounding from layer F (base and top) result in two average ages which are statistically equivalent (210 ± 28 ka and 221 ± 21 ka, respectively) (Table 2). Even if these results seem coherent, one must note that layer F was subjected to extensive chemical diagenesis that resulted in the breakdown of the clays and the formation of authigenic silica, as demonstrated by Weiner et al. (2002). As discussed by these authors, this process might be related to the erosional unconformity that marks the geological limit between the top of layer F and the bottom of E, and indicates a period of abundant water flow, especially at the entrance of the cave where the Deep Sounding is located. Indeed, the fine-bedded nature of the sediments exposed in the Deep Sounding, indicate deposition in standing water. Because clays and other mineral components are altered to a depth of more than 2 m below the erosional unconformity in this area, one cannot rule out the possibility of an increase of the γ-dose-rate leading to an under-estimation of the true deposition age. However, it is of interest that the overlaying layer (Lower E) does not show signs of such an alteration in this area and is dated to 186 ± 20 ka. It can then be deduced that the alteration was limited in time to Oxygen Isotope Stage 7 (OIS-7), from 244 to 190 ka (Martinson et al., 1987). In order to assess the magnitude of this possible under-estimation, one can consider as an extreme hypothesis that the environmental dose-rate in the Deep Sounding during OIS-7 was as low as those recorded in areas where the CD assemblage has been identified (~500 μGy/a). Considering the data of Table 1, it can then be shown that such a scenario would lead to average ages of 224 ± 29 ka and 231 ± 22 ka for layer F (base and top, respectively). Thus, the age of layer F (~210–220 ka) is possibly under-estimated but it is likely that this under-estimation does not exceed 20 ka and is similar in magnitude to the errors associated with the mean ages.

Moving up in the stratigraphic sequence, the TL age of Lower E in the Deep Sounding is 186 ± 20 ka. This is statistically indistinguishable from the average values obtained from the southern part of the Central Area for units 5 and 4 (160 ± 22 ka and 168 ± 21 ka, respectively), and is consistent with the fact that these two units were both identified as

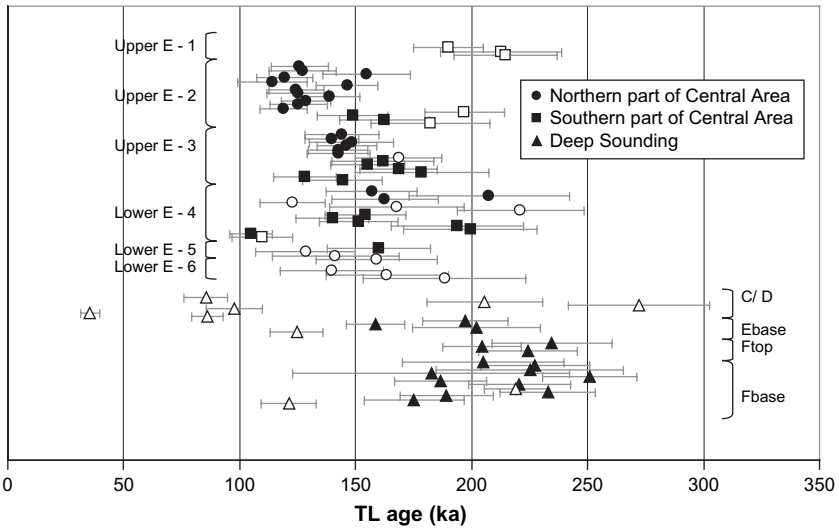

Fig. 7. All the TL age estimates obtained for the different sectors of the cave (northern and southern part of Central Area, Deep Sounding) are plotted as a function of the stratigraphy. The selected samples are represented with filled symbols, whereas open symbols indicate the discarded samples.

belonging to the Lower E complex and thus are expected to have the same age. This result is also close to the average age of unit 4 (176 ± 26 ka) in the northern part. Lower E was thus deposited at the beginning of OIS-6, a period which seems to have been much drier than the previous one according to the state of preservation of the contemporaneous units, especially in the Deep Sounding area, where these upper sediments are less diagenetically altered and commonly calcitic.

In the southern part of the Central Area, unit 3 is dated to 156 ± 19 ka, indicating that the deposition of Upper E sediments followed those of Lower E without any interruption. The dating of two samples assumed in the field to be derived from unit 2 in this part, yielded a mean TL age (156 ± 17 ka) indistinguishable from those of unit 3. We assume therefore that unit 2 was not present in the dated southern part of the Central area. In reality the correlations between the top of the Mousterian deposits in the southern section and those of the northern section were difficult to establish due to their removal by the Natufian and Aurignacian occupations and the earlier excavations of this area (1971–1979). In addition, the dipping of the units in the northern section, possibly into a sinkhole in the rear, was the reason for erroneous field correlations. Units 3 and 2 were TL-dated in the northern part and the age estimates are 144 ± 14 and 129 ± 13 ka, respectively. These last two results then show a clear-cut correlation with the stratigraphy indicating a deposition of these units in the second part of OIS-6.

6. Discussion and conclusions

We first compare the TL chronology with the most complete and reliable age data published to date for Hayonim Cave, namely from the combined ESR/U-series analyses (Rink et al., 2004). The mean TL dates obtained for units 3–5 in the southern part of the Central Area, when taking into account the standard deviations, range from ~135 ka to ~185 ka. The TL dates are therefore in fairly good agreement with the ESR dates on teeth of the same units (Early uranium Uptake model [EU]: 177 ± 12 ka and Linear uranium Uptake model [LU]: 182 ± 15 ka). The mean TL age of 156 ± 19 ka obtained for the uppermost unit (unit 3) also fits well with the U-series age of a fallen calcite speleothem ($155.3 + 2.9 - 1.4$ ka) found at a higher elevation ($Z = 248$) than all the dated samples. It can thus be concluded that the Mousterian sequence in the southern part of the Central Area, including layers Lower E (units 5 and 4) and Upper E (unit 3), covers a minimum time interval ranging from ~185 ka to ~135 ka ago. This range is reproduced in the northern part for units 4–3 including the base of E in the Deep Sounding, but in the north the youngest unit (2) is also present with an age of 129 ± 13 ka.

The dating of the erosional unconformity observed between layer F and Lower E at Hayonim Cave is of particular interest. According to the TL results, it is dated to ~200 ka and thus corresponds to the second part of OIS-7. This event was marked by significant flow of water within the cave. It might then be contemporaneous with one of the discontinuities recorded in the sequence of Tabun cave that were already described (Jelinek, 1982; Jelinek et al., 1973; Mercier et al., 1995b). An important discontinuity between Unit I dated to 165 ± 16 ka and Unit II dated to 196 ± 21 ka (Mercier and Valladas, 2003) reflects the introduction of the *terra rosa* soil due to the opening of the chimney. Earlier unconformities were noted in the stratigraphy of the inner chamber where units II–VIII accumulated following the deposition of Unit IX (Jelinek, 1982, p.1370). Units II–IX were attributed to what was originally called layer D by Garrod. The TL dates of these units are as follows: Unit V, 222 ± 27 ka; Unit IX, 256 ± 26 ka (Mercier and Valladas, 2003). Hence, the gap between Hayonim Lower E and F (both corresponding in their industries to the generalized Layer D at Tabun) would fall between Unit II and Unit V and not as mentioned in a previous paper (Weiner et al., 2002).

If these discontinuities represent the same series of climatic events, they seem to appear at the same position within the

Table 2
List of the selected samples with their TL dates and associated errors

Layer	Unit	Mean TL age (ka)	±	Sample lab. no.	Square	Location	Individual age (ka)	±	Sample lab. no.	Square	Location	Individual age (ka)	±
Northern part of Central Area													
Upper E	2	129	13 (12)	21	G18	(56,74,360)	126	12	27	G24	(70,72,400)	124	12
				24	G19	(64,27,386)	127	14	63	G25	(77,43,409)	125	13
				23	G20	(55,66,386)	155	19	26	G26	(95,75,409)	139	13
				22	G21	(70,87,394)	119	12	61	G27	(84,36,411)	129	11
				62	G22	(89,36,396)	114	15	25	G28	(60,72,418)	125	12
				20	G23	(89,74,396)	146	13	9	G19	(53,62,402)	119	10
Upper E	3	144	14 (3)	3	H19	(90,80,390)	144	16	11	H19	385-400	146	13
				5	H19	(80,55,395)	140	11	4	H19	(61,29,399)	142	13
				10	H19	(70,26,395)	148	18	7	H19	(52,40,407)	143	14
Lower E	4	176	26 (28)	415	I20	(95,95,465)	157	19	417	I20	(58,25,463)	163	23
				416	I20	(48,2,463)	208	35					
Southern part of Central Area													
Upper E	2	156	17 (10)	67	K24	(62,96,307)	149	15	68	K24	(72,62,310)	163	19
	3	156	19 (18)	65	K24	(82,37,351)	162	22	75	I24	375-380	178	29
				84	J24	(41,21,395)	155	16	82	I24	(62,42,395)	128	14
				76	I24	(46,90,371)	169	17	80	I24	(75,20,399)	144	17
Lower E	4	168	21 (27)	401	K24	(81,86,459)	154	17	403	I24	(80,57,458)	194	28
		157[a]	35 (19)	418	I24	(10,52,454)	140	16	410	K23	(7,37,457)	200	29
				402	I24	(24,1,456)	151	17	412	K22	(10,15,460)	105	9
	5	160	22 (22)	414	K23	(22,73,466)	160	22					
Deep Sounding													
Lower E	E base	186	20 (24)	58	E27	520-525	197	18	406	F28	(75,35,520)	202	28
				409	E28	(80,70,558)	159	13					
F	F top	221	21 (16)	50	E27	(45,62,545)	235	26	57	E27	(76,14,578)	224	21
				60	E27	555-560	204	17					
	F base	210	28 (25)	516	F28	(10,75,728)	205	35	526	F28	(4,95,715)	187	20
				522	F28	(23,5,719)	227	24	527	F28	(19,87,711)	221	22
				523	F28	(67,60,726)	225	41	518	F27	(54,60,733)	233	20
				524	F28	(26,14,715)	183	60	519	F27	(47,77,718)	189	20
				525	F28	(43,98,703)	251	20	520	F27	(74,98,718)	175	22

The mean ages and deviations for the indicated Mousterian layers were calculated by averaging the individual dates and errors, respectively. The standard deviations are also given.

[a] Sample no. 412 gave a young date in comparison to other results, something hard to explain.

Levantine Mousterian sequence. In Hayonim Cave, the boundary is situated between layers F and Lower E, both of which contain blade-rich Middle Paleolithic industries. Consequently, by comparing the chronologies and industries of Hayonim and Tabun caves, one can conclude that the former sequence is likely more continuous than that of Tabun and that the latter site was probably unoccupied during the first part of OIS-6. It should be noted that subsidence is more dramatic in Tabun which also may explain gaps in the physical stratigraphic record.

In sum, this study shows that the age of the Mousterian sequence in Hayonim Cave ranges from about 115 ka ago to at least 220 ka. It also shows that the dating of samples such as flints or teeth by dosimetric methods can be severely affected by the proximity of mineral assemblage boundaries to the samples and/or to the dosimeters used to measure the current radiation dose. Without three-dimensional information on the distributions of these mineral assemblages in the sediments, the ages of the stratigraphic units in Hayonim Cave would have been determined with much less precision and confidence than those presented here, and would have certainly been less reliable.

Acknowledgements

We thank the National Science Foundation, Washington (grants awarded to O. Bar-Yosef and M.C. Stiner), the French Ministry of Foreign Affairs (grants awarded to B. Vandermeersch), the Israel Science Foundation (grants awarded to S. Weiner), the American School of Prehistoric Research, Peabody Museum, Harvard University, for funding the project at Hayonim cave and the ensuing laboratory analyses. S. Weiner (the Dr Walter and Dr Trude Borchardt Professorial Chair in Structural Biology) is grateful for the generous donation by Mr George Schwartzman.

References

Aitken, M.J., 1985. Thermoluminescence Dating. Academic Press, London, 359 pp.

Arensburg, B., 2002. Human remains from Geula Cave, Haifa. Bulletins et Mémoires de la Société d'Anthropologie de Paris 14, 141–148.

Arensburg, B., Nathan, H., Mousterian, A., 1980. Third cervical vertebra from Hayonim Cave, Israel. Journal of Human Evolution 9, 193–195.

Arensburg, B., Bar-Yosef, O., Belfer-Cohen, A., Rak, Y., 1990. Mousterian and Aurignacian human remains from Hayonim Cave, Israel. Paléorient 16, 107–109.

Arensburg, B., Belfer-Cohen, A., 1998. Sapiens and Neandertals: rethinking the Levantine Middle Paleolithic Hominids. In: Akazawa, T., Aoki, K., Bar-Yosef, O. (Eds.), Neandertals and Modern Humans in Western Asia. Plenum Press, New York and London, pp. 311–322.

Bar-Yosef, O., 1991. The archaeology of the Natufian layer at Hayonim Cave. In: Bar-Yosef, O., Valla, F.R. (Eds.), The Natufian Culture in the Levant. International Monographs in Prehistory, Ann Arbor, MI, pp. 81–93.

Bar-Yosef, O., 1998. Chronology of the Middle Paleolithic of the Levant. In: Akazawa, T., Aoki, K., Bar-Yosef, O. (Eds.), Neandertals and Modern Humans in Western Asia. Plenum Press, New York and London, pp. 39–56.

Bar-Yosef, O., Belfer-Cohen, A., Goldberg, P., Kuhn, S., Meignen, L., Weiner, S., Vandermeersch, B., 2006. Archaeological background to Hayonim cave and Meged rockshelter. In: Stiner, M. (Ed.), The Faunas of Hayonim Cave (Israel): A 200 000-year Record of Paleolithic Diet, Demography and Society. American School of Prehistoric Research, Peabody Museum, Harvard University, Cambridge.

Goldberg, P., Bar-Yosef, O., 1998. Site formation processes in Kebara and Hayonim Caves and their significance in Levantine Prehistoric Caves. In: Akazawa, T., Aoki, K., Bar-Yosef, O. (Eds.), Neandertals and Modern Humans in Western Asia. Plenum Press, New York and London, pp. 107–125.

Hovers, E., 1997. Variability of Levantine Mousterian assemblages and settlement patterns: implications for understanding the development of human behavior. PhD thesis, Hebrew University.

Hovers, E., Rak, Y., Lavi, R., Kimbel, W.H., 1995. Hominid remains from Amud Cave in the context of the Levantine Middle Paleolithic. Paléorient 21 (2), 47–62.

Huxtable, J., Aitken, M.J., 1988. Datation par thermoluminescence. In: Tuffreau, A., Sommé, J. (Eds.), Le Gisement Paléolithique Moyen de Biache-Saint-Vaast (Pas de Calais), Stratigraphie, Environnement, Études Archéologiques, Vol. I. Memoires de la Société Préhistorique Française XXI, pp. 107–108.

Jelinek, A.J., 1981. The Middle Paleolithic in the Southern Levant from the perspective of the Tabun Cave. In: Cauvin, J., Sanlaville, P. (Eds.), Préhistoire du Levant, Chronologie et Organisation de l'Espace Depuis les Origines jusqu'au VIème Millénaire. Colloques internationaux du CNRS, no. 598. Editions du CNRS, Paris, pp. 265–280.

Jelinek, A.J., 1982. The Tabun cave and Paleolithic man in the Levant. Science 216, 1369–1375.

Jelinek, A.J., Farrand, W.R., Haas, G., Horowitz, A., Goldberg, P., 1973. New excavations at the Tabun Cave (Mount Carmel, Israel). Preliminary report. Paléorient 1, 151–183.

Joron, J.-L., 1974. Contribution à 1'analyse des éléments en traces dans les roches et les minéraux par activation neutronique. Application à la caractérisation d'objets archéologiques. Thèse de 3 ème Cycle, Université Paris-Sud.

Karkanas, P., Bar-Yosef, O., Goldberg, P., Weiner, S., 2000. Diagenesis in prehistoric caves: the use of minerals that form in situ to assess the completeness of the archaeological record. Journal of Archaeological Science 27, 915–929.

Liritzis, Y., Kokkoris, M., 1992. Revised dose-rate data for thermoluminescence/ESR dating. Nuclear Geophysics 6, 423–443.

Mann, A.E., 1995. Modern human origins: evidence from the Near East. Paléorient 21 (2), 35–46.

Marks, A.E., Volkman, P., 1986. The Mousterian of Ksar Akil: levels XXVIA through XXVIIIB. Paléorient 12 (1), 5–20.

Martinson, P.M., Pisias, N.G., Hays, J.D., Imbrie, J., Moore, T.C., Shackleton, N.J., 1987. Age dating and the orbital theory of the ice ages, development of a high-resolution 0 to 300,000-year old chronostratigraphy. Quaternary Research 27, 1–29.

Meignen, L., 1998. Hayonim Cave lithic assemblages in the context of the Near Eastern Middle Paleolithic: a preliminary report. In: Akazawa, T., Aoki, K., Bar-Yosef, O. (Eds.), Neandertals and Modern Humans in Western Asia. Plenum Press, New York and London, pp. 165–180.

Meignen, L., 2000. Early Middle Palaeolithic blade technology in Southwestern Asia. Acta Anthropologica Sinica 19 (Suppl.), 158–168.

Mercier, N., Valladas, H., Joron, J.-L., Reyss, J.-L., Lévêque, F., Vandermeersch, B., 1991. Thermoluminescence dating of the late Neanderthal remains from Saint-Césaire (France). Nature 351, 737–739.

Mercier, N., Valladas, H., Valladas, G., 1992. Some observations on palaeodose determination in burnt flints. Ancient TL 10 (3), 28–32.

Mercier, N., Valladas, H., Valladas, G., 1995a. Flint thermoluminescence dates from the CFR Laboratory at Gif: contributions to the study of the chronology of the Middle Palaeolithic. Quaternary Science Reviews (Quaternary Geochronology) 14, 351–364.

Mercier, N., Valladas, H., Valladas, G., Reyss, J.-L., Jelinek, A., Meignen, L., Joron, J.-L., 1995b. TL dates of burnt flints from Jelinek's excavations at Tabun and their implications. Journal of Archaeological Science 22, 495–509.

Mercier, N., Valladas, H., Joron, J.-L., Schiegl, S., Bar-Yosef, O., Weiner, S., 1995c. Thermoluminescence dating and the problem of geochemical evolution of sediments – a case study: the Mousterian Levels at Hayonim. Israel Journal of Chemistry 35, 137–141.

Mercier, N., Valladas, H., Froget, L., Joron, J.-L., Ronen, A., 2000. Datation par la thermoluminescence de la base du gisement paléolithique de Tabun (Mont Carmel, Israël). Comptes Rendus de l'Académie des Sciences 330, 731–738.

Mercier, N., Valladas, H., 2003. Reassessment of TL age-estimates of burnt flints from the Paleolithic site of Tabun Cave, Israel. Journal of Human Evolution 45, 401–409.

Neuville, R., 1951. Le Paléolithique et le Mésolithique du désert de Judée. Archives de l'Institut de Paléontologie Humaine. Mémoire no. 24. Masson et Cie, Paris.

Prescott, J.R., Hutton, J.T., 1988. Cosmic ray and gamma ray dosimetry for TL and ESR. Nuclear Tracks and Radiation Measurements 14, 223–227.

Rak, Y., 1998. Does any Mousterian cave present evidence of two Hominid species? In: Akazawa, T., Aoki, K., Bar-Yosef, O. (Eds.), Neandertals and Modern Humans in Western Asia. Plenum Press, New York and London, pp. 353–366.

Rink, W.J., Schwarcz, H.P., Weiner, S., Goldberg, P., Meignen, L., Bar-Yosef, O., 2004. Age of the Mousterian industry at Hayonim Cave, Northern Israel, using electron spin resonance and $^{230}Th/^{234}U$ methods. Journal of Archaeological Science 31, 953–964.

Shahack-Gross, R., Berna, F., Karkanas, P., Weiner, S., 2004. Bat guano and preservation of archaeological remains in cave sites. Journal of Archaeological Science 31, 1259–1272.

Schiegl, S., Lev-Yadun, S., Bar-Yosef, O., El Goresy, A., Weiner, S., 1994. Siliceous aggregates from prehistoric wood ash: a major component of sediments in Kebara and Hayonim caves (Israel). Israel Journal of Earth Sciences 43, 267–278.

Schiegl, S., Goldberg, P., Bar-Yosef, O., Weiner, S., 1996. Ash deposits in Hayonim and Kebara Caves: macroscopic, microscopic and mineralogical observations, and their archaeological implications. Journal of Archaeological Science 23, 763–781.

Schwarcz, H.P., Goldberg, P., Blackwell, B., 1980. Uranium series dating of archaeological sites in Israel. Israel Journal of Earth Sciences 29, 157–165.

Schwarcz, H.P., Rink, W.J., 1998. Progress in ESR and U-series chronology of the Levantine Paleolithic. In: Akazawa, T., Aoki, K., Bar-Yosef, O. (Eds.), Neandertals and Modern Humans in Western Asia. Plenum Press, New York and London, pp. 57–67.

Stiner, M.C., 2006. The Faunas of Hayonim Cave (Israel): A 200,000 Year Record of Paleolithic Diet, Demography and Society. American School of Prehistoric Research, Bulletin 48. Peabody Museum Press, Harvard University, Cambridge, MA.

Stiner, M.C., Munro, N.D., Surovell, T.A., 2000. The tortoise and the hare: small game use, the broad spectrum revolution, and Paleolithic demography. Current Anthropology 41 (1), 39–73.

Stiner, M.C., Kuhn, S.L., Surovell, T.A., Goldberg, P., Meignen, L., Weiner, S., Bar-Yosef, O., 2001. Bone preservation in Hayonim Cave (Israel): a macroscopic and mineralogical study. Journal of Archaeological Science 28, 643–659.

Tchernov, E., 1988. Biochronology of the Middle Palaeolithic and dispersal events of Hominids in the Levant. ERAUL 29. L'Homme de Néandertal 2, 153–168.

Tchernov, E., 1998. The faunal sequence of the southwest Asian Middle Paleolithic in relation to hominid dispersal events. In: Akazawa, T., Aoki, K.,

Bar-Yosef, O. (Eds.), Neandertals and Modern Humans in Western Asia. Plenum Press, New York and London, pp. 77–90.

Tillier, A.-M., 1998. Ontogenetic variation in Late Pleistocene *Homo sapiens* from the Near East: implications for methodological bias in reconstructing evolutionary biology. In: Akazawa, T., Aoki, K., Bar-Yosef, O. (Eds.), Neandertals and Modern Humans in Western Asia. Plenum Press, New York and London, pp. 381–389.

Tillier, A.-M., Arensburg, B., Vandermeersch, B., Chech, M., 2003. New human remains from Kebara Cave (Mount Carmel). The place of the Kebara Hominids in the Levantine Mousterian fossil record. Paléorient 29 (2), 35–64.

Trinkaus, E., 1995. Near eastern archaic humans. Paléorient 21 (2), 9–24.

Valladas, G., 1988. Stopping power and range for alpha particles in SiO_2. Ancient TL 6, 7–8.

Valladas, H., 1992. Thermoluminescence dating of flint. Quaternary Science Reviews 11, 1–5.

Valladas, G., Valladas, H., 1982. Effet de l'irradiation alpha sur des grains de quartz. A specialist seminar on thermoluminescence dating. PACT 6, 171–178.

Valladas, G., Mercier, N., Létuvé, R., 1994. A simple semi-automatic TL apparatus of new design. Ancient TL 12, 39–40.

Valladas, H., Geneste, J.M., Joron, J.L., Chadelle, J.P., 1986. Thermoluminescence dating of Le Moustier (Dordogne, France). Nature 322, 452–454.

Valladas, H., Joron, J.-L., Valladas, G., Arensburg, B., Bar-Yosef, O., Belfer-Cohen, A., Goldberg, P., Laville, H., Meignen, L., Rak, J., Tchernov, E., Tillier, A.-M., Vandermeersch, B., 1987. Thermoluminescence dates for the Neanderthal burial site at Kebara in Israel. Nature 330, 159–160.

Valladas, H., Reyss, J.-L., Joron, J.-L., Valladas, G., Bar-Yosef, O., Vandermeersch, B., 1988. Thermoluminescence dating of Mousterian 'Proto-Cro-Magnon' remains from Israel and the origin of modern man. Nature 331, 614–616.

Valladas, H., Mercier, N., Joron, J.-L., Reyss, J.-L., 1998. Gif Laboratory dates for Middle Paleolithic Levant. In: Akazawa, T., Aoki, K., Bar-Yosef, O. (Eds.), Neandertals and Modern Humans in Western Asia. Plenum Press, New York and London, pp. 69–75.

Vandermeersch, B., 1995. Le rôle du Levant dans l'évolution de l'humanité au Pléistocène supérieur. Paléorient 21 (2), 25–34.

Weiner, S., Goldberg, P., Bar-Yosef, O., 1993. Bone preservation in Kebara Cave, Israel, using on-site Fourier-transform infrared spectrometry. Journal of Archaeological Science 20, 613–627.

Weiner, S., Goldberg, P., Bar-Yosef, O., 2002. Three-dimensional distribution of minerals in the sediments of Hayonim Cave, Israel: diagenetic processes and archaeological implications. Journal of Archaeological Science 29, 1289–1308.